

The effect of wind farming on mesocale flow

Validation and prediction

A.J. Brand

This report has been presented at:

- the European Wind Energy Conference 2009, Marseille, France, 16-19 March 2009;
- IEA Wind Task 23 Back-to-back Workshop "Offshore wind farms - Wake effects and power fluctuations", Risø-DTU, Risø campus, Denmark, 25-26 February 2009;
- We-at-sea/ATO/NWEA Offshore Wind Energy Conference "Essential innovations", Den Helder, Netherlands, 12-13 February 2009

ECN-M--09-051

The effect of wind farming on mesoscale flow - Validation and prediction

Arno J Brand

ECN Wind Energy, P.O. Box 1, NL 1755 ZG Petten, Netherlands

E: brand@ecn.nl, T: +31 224 56 4775, F: +31 224 56 8214

Abstract

This paper addresses validation of the planetary boundary layer method MFwWF and predictions as obtained with MFwWF. The validation considers measured wind farm wakes. The predictions include the modification of the wind profile due to wind farming plus the impact of wind farm design parameters and meteorological parameters on the wind profile.

A validation of MFwWF is presented on basis of velocities measured downstream of the Horns Rev and the Nysted wind farms. The calculated decrease of the relative velocity deficit with increasing distance downstream a wind farm is supported by measured data from both wind farms. As to the calculated decrease of this deficit with increasing upstream velocity the measured data is inconclusive. Quantitative conclusions have not been drawn because the calculations and the measurements are evaluated in different spanwise positions. In a qualitative sense the calculated relative velocity deficits are in agreement with the measured ones.

Resolved profiles show how most of the velocity change occurs in the lower part of the boundary layer whereas most of the wind direction change occurs in the upper part, and that the thinner the boundary layer or the larger the surface roughness, the larger the wind direction change. Near a 5 MW wind turbine with a rotor diameter of 100 m operating at full load the velocity deficit is of the order of 5%, the wind direction change is increased with 1...2 deg, and the velocity recovery distance is 20 rotor diameters. For a wind farm with 22 of these turbines separated at 10 rotor distances these numbers are 15%, 2...3 deg, and at least 2 wind farm length scales.

Initial velocity deficits and velocity recovery distances show the impact of nominal power density and geostrophic velocity for a wind farm which consists of 22 wind turbines with a nominal power of 5 MW. The initial velocity deficit relative to the upstream velocity decreases with increasing geostrophic velocity in general, and ranges from 6% (at a turbine separation of 14 rotor diameters) to 32% (at a separation of 5 rotor diameters) if the velocity at hub height is halfway cut-in and nominal. At this hub-height velocity the absolute initial velocity deficit reaches a maximum (of 1.2 m/s in the case of a nominal power density of 5 MW/km²) and the velocity recovery

distance relative to the wind farm length scale is of the order of 20. The relative velocity recovery distance for other geostrophic velocities varies between 0 (at low geostrophic velocities) and a limit value of the order of 40 (at high velocities).

Key words Wind farm wake, Wind resource assessment

1. Introduction

Offshore wind farms tend to be placed closer together over the years, as already illustrated by Offshore Windfarm Egmond aan Zee OWEZ and Princess Amalia Wind Farm (separated 15 km) in the Netherlands or Horns Rev I and II (separated 23 km) in Denmark. Since these separation distances are between 5 and 10 times the wind farm's horizontal length scale, the velocity deficit due to an upstream wind farm may be considerable [1]. If so, energy production loss and mechanical load increase are expected to be significant. For this reason the dedicated planetary boundary layer method Mesoscale Flow with Wind Farming (MFwWF) has been developed, which method computes the interaction between a wind farm and the prevailing wind. The methodology behind MFwWF and predictions obtained with MFwWF have been reported separately [2][3][4].

In this paper we address validation of MFwWF and predictions obtained with MFwWF. We start with brief descriptions of prior work on modelling wind farm wakes (section 2) and the new dedicated planetary boundary layer method MFwWF (section 3). Next validation on basis of measured wind farm wakes is addressed (section 4). We then present predictions in the form of the modification of the wind profile due to wind farming plus the impact of wind farm design parameters and meteorological parameters on the wind profile (section 5). Finally, we summarize the findings (section 6).

2. Prior work

The mean (in the sense of Reynolds averaged) flow in the neutral planetary boundary layer usually is described by the momentum equations in combination with the continuity equation and a set of boundary conditions [5]. These momentum equations represent equilibrium between convective forces, pressure gradient forces, Coriolis

forces, forces due to turbulent flux gradients, and external forces.

A wind farm wake study requires simulation of mesoscale atmospheric flow together with energy extraction/redistribution due to wind turbines. The studies that have been published so far can be subdivided into two categories: self-similar approaches and mesoscale approaches. In a self-similar approach [6] [7] the convective force and the spanwise turbulent momentum flux gradients are assumed to dominate the flow, allowing for standard wake-like solutions. In a mesoscale approach, on the other hand, the flow is assumed to be dominated by the Coriolis force and the vertical turbulent momentum flux gradients, opening the door to either extra surface drag approaches [8] or more generic mesoscale approaches [9][10][11]. As is shown in other publications [2][3], neither the self-similar wake approach nor the extra surface drag approach is valid on the mesoscale because over the separation distance between wind farms the convective and the Coriolis forces are of equal order of magnitude so that neither can be neglected. Although this was already implicitly recognized in the more generic approaches, these studies lack realistic formulations for the turbulence and the wind turbines.

3. Flow model

3.1. Principles and outline of method

This subsection presents a brief description of the planetary boundary layer method MFwWF; details have been reported elsewhere [2][3].

MFwWF is a CFD method that is based on three principles:

- (1) Neutral planetary boundary layer flow with wind farming essentially is steady and two-dimensional. In addition the convective forces, the Coriolis forces, the vertical and spanwise gradients of the turbulent momentum fluxes, and the external forces that represent wind turbines all have the same order of magnitude.
- (2) A numerical representation of the momentum equations in the form of backward differences allows for
 - (a) an implicit solution of the two horizontal velocity components in vertical direction, iterating on the turbulent viscosity while employing a mass-energy conserving scheme, and
 - (b) a marching solution in the horizontal directions.
- (3) The continuity equation is satisfied by employing the Lagrange multiplier method to the velocity components that satisfy the continuity equation.

Because of its mixed implicit/explicit character, the planetary boundary layer method MFwWF is computationally fast and cheap.

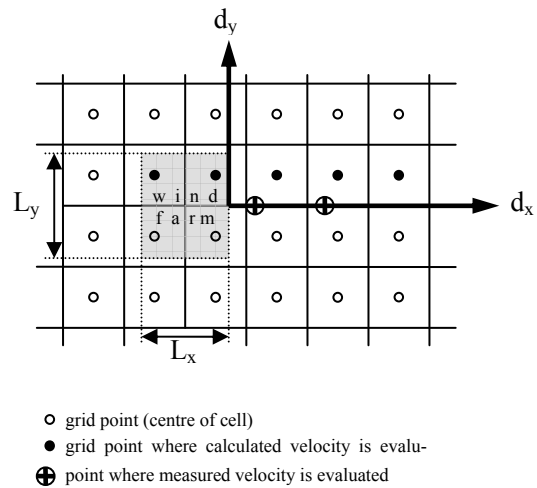


Figure 1: Horizontal lay-out of the grid cells in relation to the horizontal area covered by the wind farm, and definition sketch of downstream distance d_x , spanwise distance d_y , streamwise wind farm length scale L_x and spanwise wind farm length scale L_y . Also indicated are the points where measured velocity is evaluated in the validation study

Apart from the hub height and power curve of the turbines in the wind farm and information on the location and the lay-out of the wind farm, the input to the planetary boundary layer method MFwWF includes the geostrophic velocity, the geostrophic height (i.e. the height where the geostrophic velocity is reached) and the surface roughness length (i.e. the height where the velocity is zero).

The output of MFwWF consists of the grid-cell-averaged values of the two horizontal velocity components and the turbulent viscosity. The turbulent viscosity is modeled with a Baldwin-Lomax model [12] which is modified such that realistic values of the velocity and the turbulence intensity at heights between 10 m and 100 m are obtained.

Figure 1 shows the horizontal lay-out of the grid cells in relation to the horizontal area covered by the wind farm. Also indicated in figure 1 are the locations where measured velocity is evaluated in the validation study (section 4); note these are at a different spanwise location.

3.2. Numerical stability

In this subsection we briefly address the numerical stability of the solution procedure in MFwWF. To this end consider the matrix-vector representation of the discretized momentum equations. Now in general an error in a matrix element will propagate into an error in the resolved vector. In order to prevent instability we require that the absolute value of the growth rate remains smaller than 1.

At the bottom of the numerical domain, where errors grow from initial velocities $u \approx 0$ and $v \approx 0$, we have shown that this requirement is met if

$$\frac{\min(\Delta x, \Delta y)}{\Delta z_{\min}^4} \geq c_{b1} \frac{f_{\phi} \max(|u_g|, |v_g|)}{k_m^2(z_0)}$$

where Δx and Δy indicate the horizontal grid spacings, Δz_{\min} indicates the spacing between the lower two points in vertical direction, c_{b1} indicates a constant of proportionality, f_{ϕ} is the Coriolis parameter, u_g and v_g are the streamwise and the spanwise component of the geostrophic velocity, and $k_m(z_0)$ indicates the turbulent viscosity at the bottom of the numerical domain. This means that for the solution procedure to remain stable the horizontal grid sizes must be larger than a critical value which is proportional to the vertical grid size and the value of the Coriolis parameter, and which is inversely proportional to the turbulent viscosity.

At the top of the numerical domain, on the other hand, errors grow from initial velocities $u \approx u_g$ and $v \approx v_g$, and we have shown that the requirement on preventing error propagation is met if

$$\frac{\min(2\Delta x - \Delta y, 2\Delta y - \Delta x)}{\Delta z_{\max}^2} \geq c_{t1} \frac{\max(|u_g|, |v_g|)}{k_m(h_{\text{geo}})}$$

where Δz_{\max} indicates the spacing between the upper two points in vertical direction, c_{t1} indicates a constant of proportionality and $k_m(h_{\text{geo}})$ is the turbulent viscosity at the top of the numerical domain.

As an illustration of the stability requirements figure 2 shows the empirically determined minimal horizontal grid size for different combination of the geostrophic height and the surface roughness length in the case of a geostrophic wind speed of 14.1 m/s.

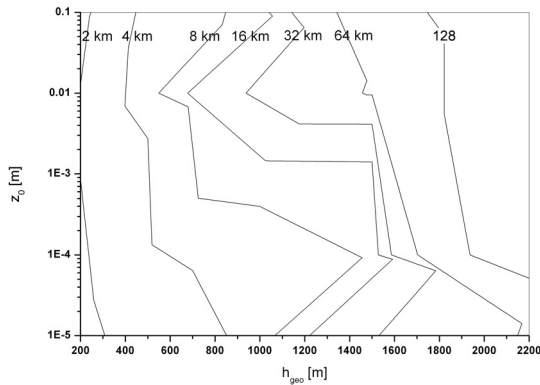


Figure 2: Smallest horizontal grid spacing if the solution procedure is to remain stable as a function of geostrophic height h_{geo} and surface roughness length z_0

4. Validation

In this section we address validation of the planetary boundary layer method MFwWF. Validation data consists of 10-minute averaged velocities measured at or near hub height at met masts located upstream and downstream of the Horns Rev wind farm and the Nysted wind farm. Note that in both cases the velocity is measured along

the central wind turbine row, which implies that measured and calculated velocities are evaluated at different spanwise positions in this study (see figure 1).

The Horns Rev wind farm consists of 80 wind turbines with a hub height of 70 m, a rotor diameter of 80 m and a nominal power of 2 MW. It covers an area of approximately 20 km², and has wind turbine rows directed 90-270 deg (from West to East). The Nysted wind farm, on the other hand, consists of 72 wind turbines with a hub height of 69 m and a rotor diameter of 84 m. These turbines can operate at two modes, reaching the full nominal power of 2.3 MW at one mode but a lower nominal power of 0.4 MW at the other. Nysted covers an area of approximately 23 km², and has rows directed 98-278 deg.

Figure 3 shows the velocity W relative to the upstream velocity W_{ups} as a function of the downstream distance d_x from the Horns Rev wind farm for upstream velocities of 6 m/s, 8 m/s and 10 m/s in combination with wind directions between 255 deg and 285 deg. In the calculations the surface roughness length is 0.1 mm, the geostrophic height is 500 m, and the geostrophic velocity is set such that the correct velocity at hub height is obtained. The number of grid points in vertical direction is 100. The calculated velocities are average values in grid cells with a horizontal area of 3.92 x 3.92 km² and the centre at a spanwise distance of 1.96 km at a height of 66 m. The measured velocities, on the other hand, are point values at a spanwise distance zero and at downstream distances of 2 km and 6 km at a height of 70 m. Upstream turbulent intensities have the same order of magnitude in the calculations and in the measurements (10% resp. between 7% and 8%).

The data in figure 3 clearly show that the calculated relative velocity deficit $(W_{\text{ups}} - W)/W_{\text{ups}}$ is smaller than the measured one. This is explained by the different spanwise positions of the points where calculated and measured velocity are evaluated in combination with the different character of these velocities (cell averaged versus point value). There however is qualitative agreement in the sense that the relative velocity deficit decreases with downstream distance. Figure 3 also shows that at a spanwise distance d_y of 0 km relative velocity deficits of 15...17% have been measured at a downstream distance of 2 km, and 7...10% at 6 km. This means that for a given downstream distance and upstream velocity between 6 m/s and 10 m/s the measured relative velocity deficit is proportional to the upstream velocity. In contrast, at a spanwise distance d_y of 1.96 km (which corresponds to $d_y/L_y = 0.50$ where L_y is the spanwise length scale of the wind farm), the calculated relative velocity deficits are found to decrease with increasing upstream velocity, with values in the range 14...13% at a d_x of 2 km

and 5...4% at 6 km (first value corresponds to the lower upstream velocity).

Calculations with higher values of the surface roughness length and/or the geostrophic height did not give significantly different results.

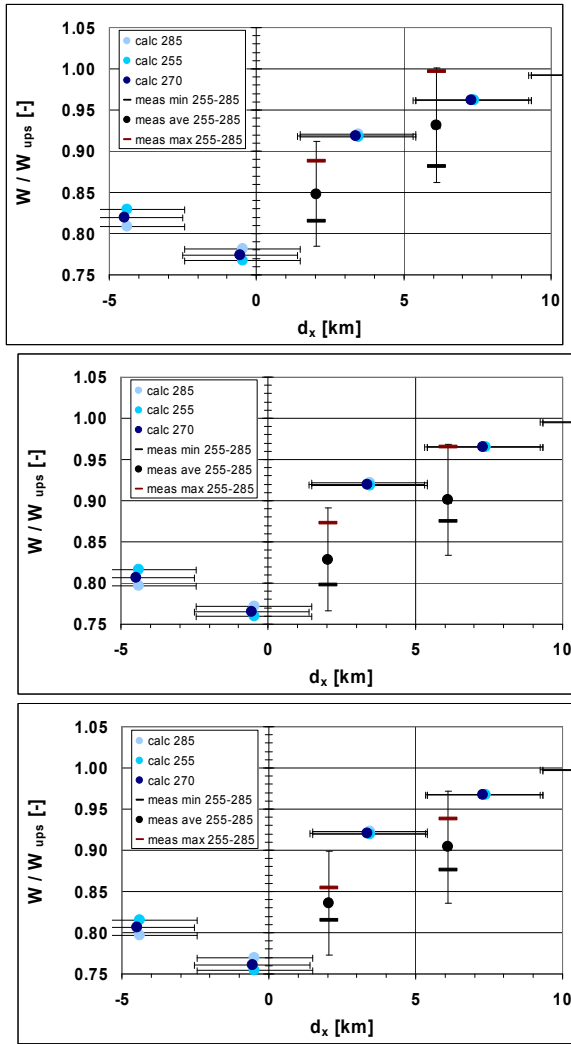


Figure 3: Velocity W relative to the upstream velocity W_{ups} as a function of distance d_x downstream the Horns Rev wind farm; upstream velocity 6 m/s (top), 8 m/s (centre) and 10 m/s (bottom). Calculated grid cell averaged velocities are presented for three different wind directions: aligned with turbine rows (wind direction 270 deg) and misaligned over ± 15 deg (285 resp. 255 deg). Horizontal error bars indicate the size of the grid cell. Bold vertical error bars indicate the minimum and the maximum of the point measurements. As a reference thin vertical error bars show a variation of 7.5% about the average of the point measurements

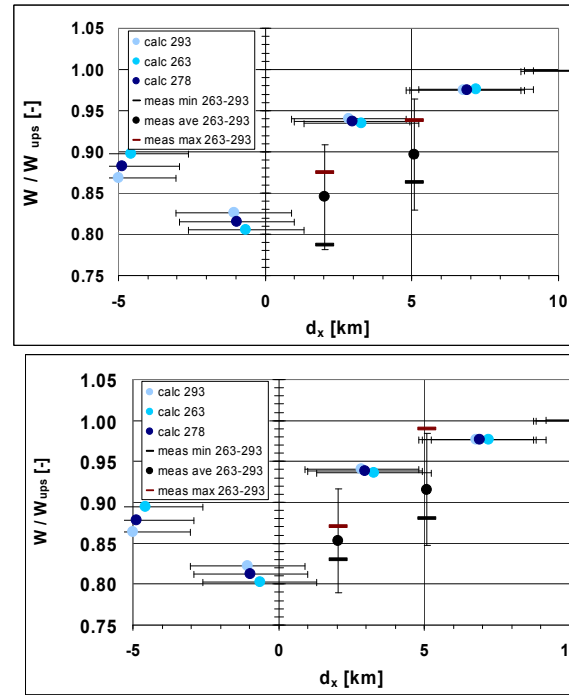


Figure 4: Velocity relative to the upstream velocity as a function of distance downstream the Nysted wind farm; upstream velocity 8 m/s (top) and 10 m/s (bottom). Calculated velocities are presented for three different wind directions: aligned with turbine rows (wind direction 278 deg) and misaligned over ± 15 deg (293 resp. 263 deg). See caption of figure 3 for interpretation of error bars

Figure 4 shows the same information for the Nysted wind farm for upstream velocities of 8 m/s and 10 m/s in combination with wind directions between 263 deg and 293 deg. Apart from the wind turbine and the wind farm data the input to the calculations is the same as for the Horns Rev case, which however implies that the calculations are evaluated at $d_y/L_y = 0.49$ as the Nysted wind farm has a smaller spanwise length scale. The velocities are measured at downstream distances of 2 km and 5 km at a height of 69 m. Measured upstream turbulent intensity is between 7% and 9%.

The data in figure 4 reveal much the same information as in figure 3 but with one exception: the measured relative velocity deficits are found to decrease with increasing upstream velocity which is in agreement with the trend in the calculated velocity deficits.

In conclusion, the calculated relative velocity deficits have been found to decrease with downstream distance from a wind farm, which is in agreement with the measurements in the wake of the Horns Rev and the Nysted wind farms. Also these calculated deficits have been found to decrease with upstream velocity, which is in contrast to measured deficits from Horns Rev but in agreement with those from Nysted. Quantitative conclusions can however not be drawn because of the difference between the spanwise positions

where the calculations and the measurements are evaluated. Nevertheless, in a qualitative sense the predicted relative velocity deficits have been found to be in agreement with the measured ones because the calculated deficits (evaluated at a spanwise position of 1.95 km) are smaller than the measured deficits (evaluated at a spanwise position zero).

5. Predictions

5.1. Resolved velocity profiles

5.1.1. Empty set

In this section the resolved velocity profiles for the empty set, that is a domain without wind farming, are presented. Figure 5 shows four vertical profiles, each in a corner of a 200 x 200 km² domain, as valid for a geostrophic height of 500 m and a surface roughness length of 0.1 mm. The number of grid points in vertical direction is 25. The figures display the streamwise velocity versus height, the spanwise velocity, the angle between the streamwise and the spanwise velocity, and a hodograph of the two velocity components. The data in the figure is in qualitative agreement with the observed height dependence of undisturbed wind, where most of the velocity change occurs in the lower part and most of the direction change occurs in the upper part of the boundary layer, but it is too early to decide on the quantitative agreement.

The figures 6 and 7 display a much thicker boundary layer (1500 m) with the same surface roughness, and the same boundary layer thickness in combination with a much rougher surface (1 cm). The figures show that the thinner the boundary layer or the larger the surface roughness, the larger the twist in the velocity profile. Again this qualitative agreement with observations is to be collaborated with quantitative data.

5.1.2. Wind turbine and wind farm

The modification of the wind profile due to an hypothetical wind turbine is studied for a turbine with a nominal power of 5 MW operating at full load, and having a rotor diameter of 100 m and a hub height of 70 m. Figure 8 shows that the relative initial velocity deficit is of the order of 5% and that the velocity twist is increased with 1...2 deg. (The relative initial velocity deficit is the ratio of the velocity deficit at $d_x = 0$ and the upstream velocity.) The velocity recovery distance d_{rec} is 20 rotor diameters. This distance is the downstream distance where the velocity is 99.9% of the upstream velocity, and is determined by fitting a decay law to the velocities and the corresponding downstream distances.

The hypothetical wind farm consists of 22 turbines with a rotor diameter of 100 m, a hub height of 70 m and a nominal power of 5 MW. The turbine separation distance is 1 km (10 rotor diameters) so that the nominal power density is 5

MW/km². Figure 9 shows that if the wind farm operates at full load the initial velocity deficit is of the order of 15% and that the velocity twist is increased with 2...3 deg. The velocity recovery distance is at least 2 streamwise wind farm length scales L_x , where the streamwise length scale is equal to the length of the wind farm.

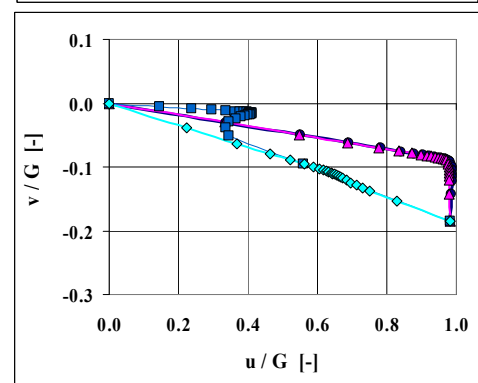
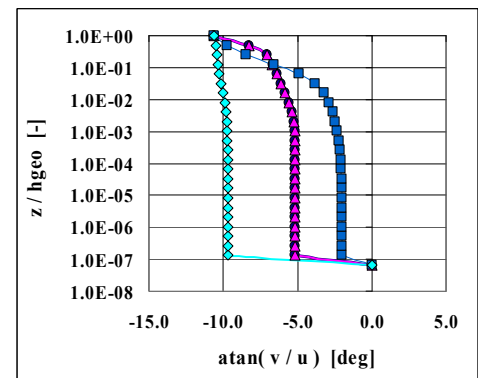
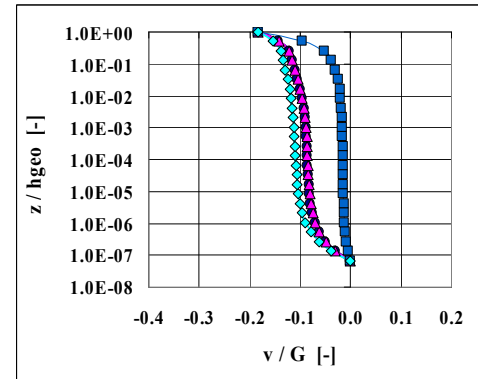
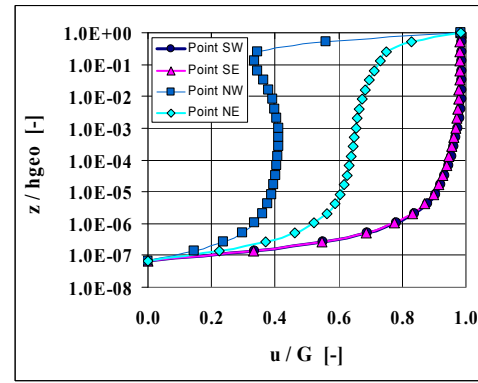
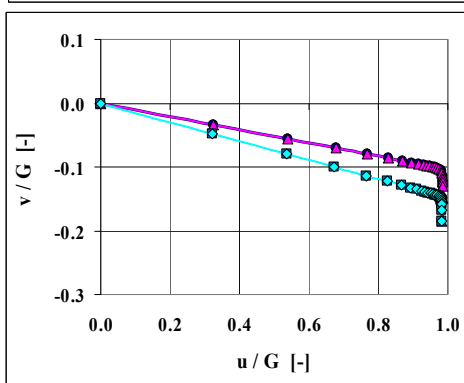
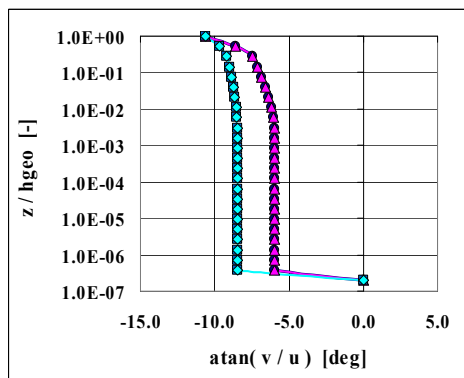
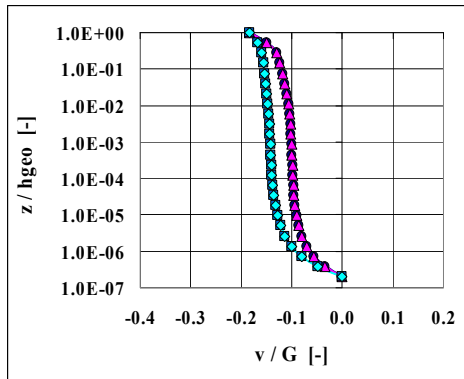
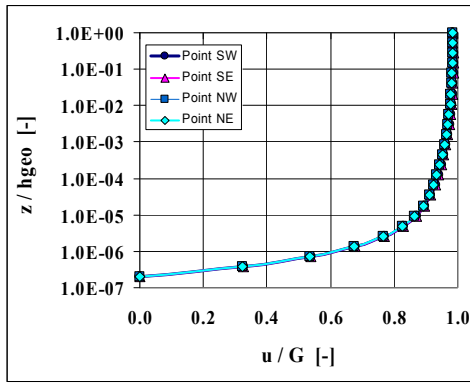


Figure 5: Vertical profiles of streamwise velocity u and spanwise velocity v in four corners of the numerical domain as non-dimensionalized with the geostrophic velocity G and the geostrophic height h_{geo} ; valid for a geostrophic height of 500 m and a surface roughness length of 0.1 mm

Figure 6: Vertical profiles of streamwise velocity u and spanwise velocity v in four corners of the numerical domain as non-dimensionalized with the geostrophic velocity G and the geostrophic height h_{geo} ; valid for a geostrophic height of 1500 m and a surface roughness length of 0.1 mm

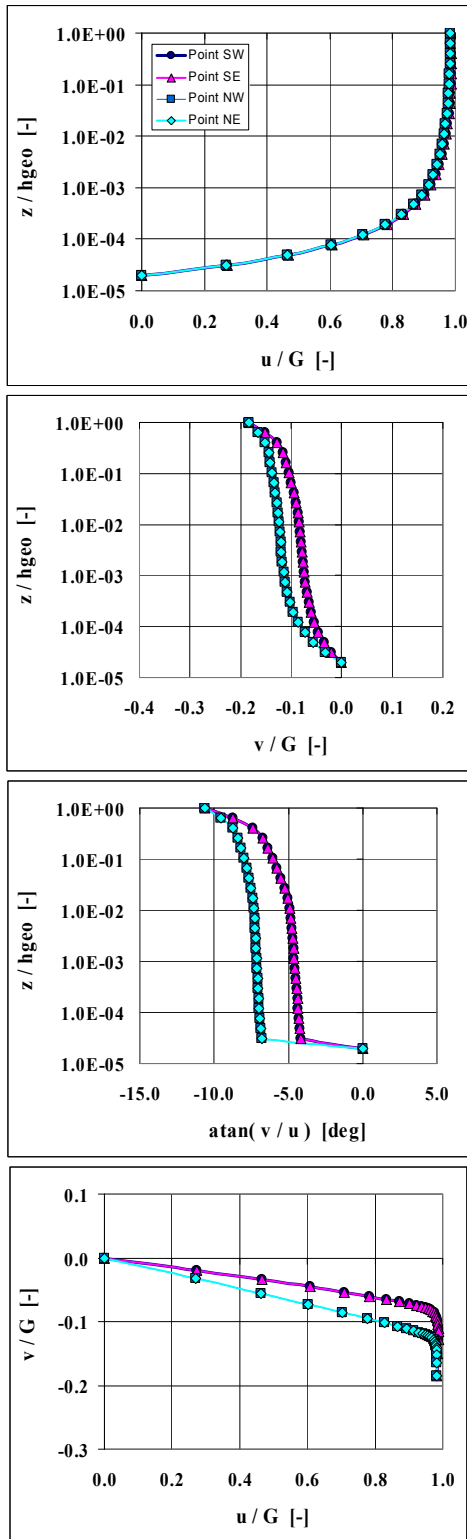


Figure 7: Vertical profiles of streamwise velocity u and spanwise velocity v in four corners of the numerical domain as non-dimensionalized with the geostrophic velocity G and the geostrophic height h_{geo} ; valid for a geostrophic height of 500 m and a surface roughness length of 1 cm

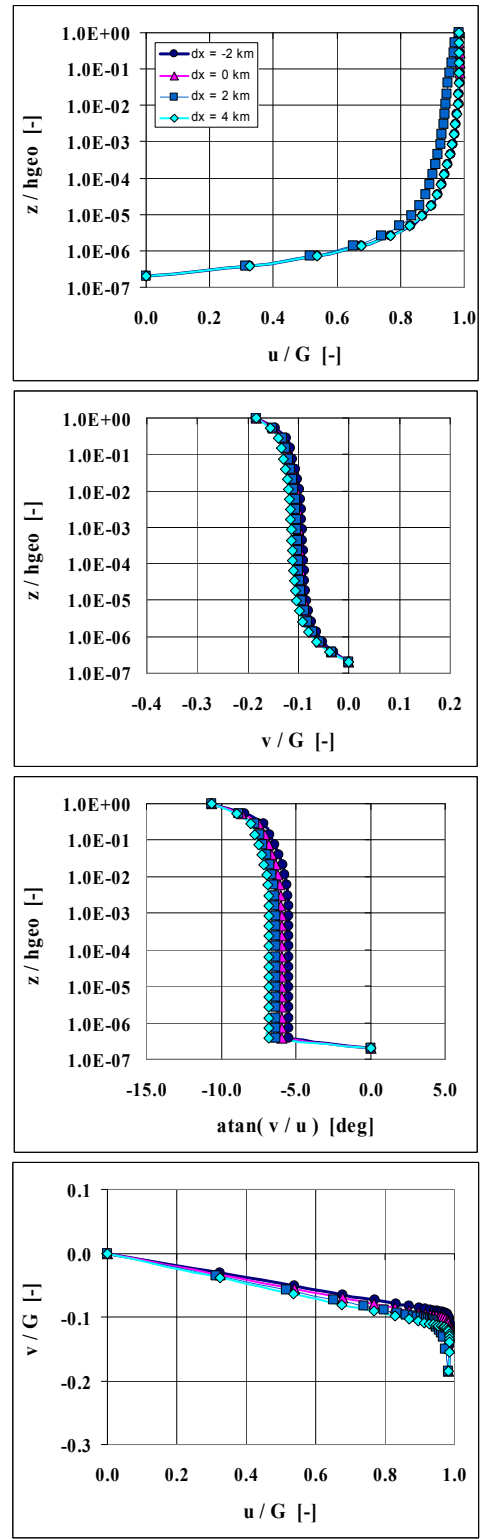


Figure 8: Vertical profiles of streamwise velocity u and spanwise velocity v for different distances d_x behind a wind turbine as non-dimensionalized with the geostrophic velocity G and the geostrophic height h_{geo} ; valid for a geostrophic height of 500 m and a surface roughness length of 0.1 mm

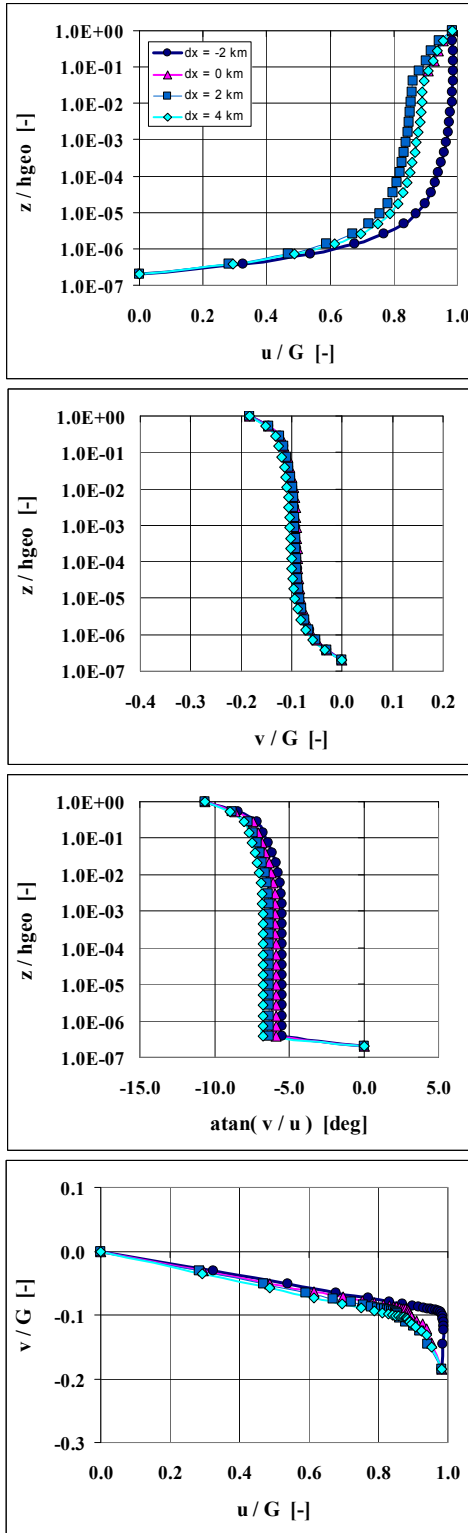


Figure 9: Vertical profiles of streamwise velocity u and spanwise velocity v for different distances d_x behind a wind farm as non-dimensionalized with the geostrophic velocity G and the geostrophic height h_{geo} ; valid for a geostrophic height of 500 m and a surface roughness length of 0.1 mm

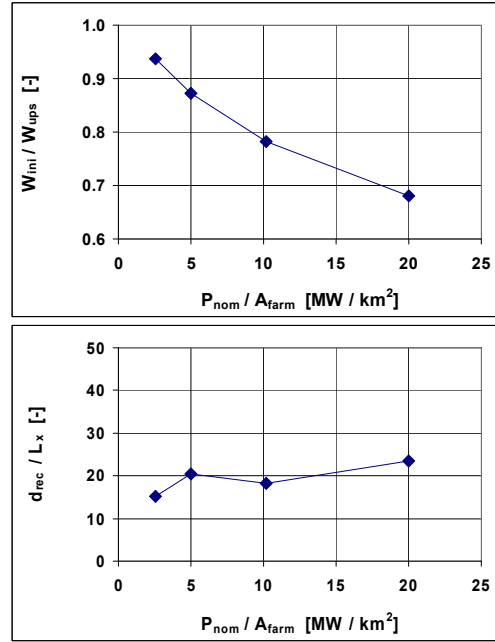


Figure 10: Initial downstream velocity W_{ini} relative to the upstream velocity W_{ups} and velocity recovery distance d_{rec} relative to the streamwise wind farm length scale L_x as a function of nominal power density P_{nom}/A_{farm} for a wind farm in a geostrophic height of 500 m, a geostrophic velocity of 14 m/s, and a surface roughness length of 0.1 mm

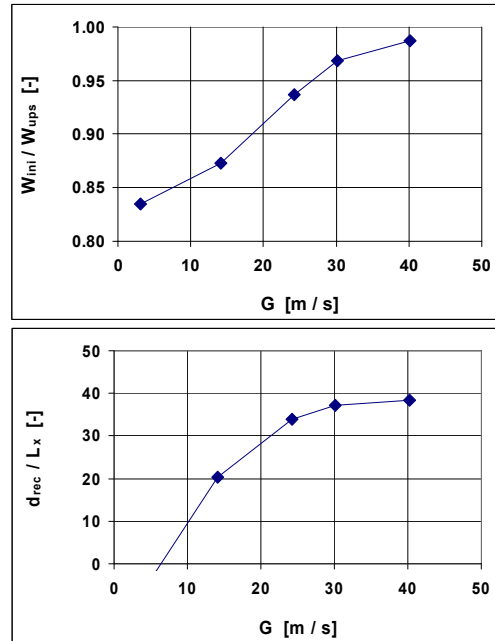


Figure 11: Initial downstream velocity W_{ini} relative to the upstream velocity W_{ups} and velocity recovery distance d_{rec} relative to the streamwise wind farm length scale L_x as a function of geostrophic velocity G for a wind farm with a nominal power density of 5 MW/km²

5.2. Impact of wind farm design parameters and meteorological parameters

Wind farm design parameters include separation distance and layout (spacing, nominal power density) of the wind farm, and hub height and rotor diameter of the wind turbine. The impact of nominal power density is studied by changing the turbine separation distance in the hypothetical wind farm between 5 and 14 times the rotor diameter and keeping the geostrophic velocity at a constant value such that the hub-height velocity is halfway cut-in and nominal. Figure 10 shows that the relative initial velocity deficit $(W_{\text{ups}} - W_{\text{ini}})/W_{\text{ups}}$ increases with the nominal power density from 6% (turbine separation 14 rotor diameters) to 32% (5 rotor diameters), and that the relative velocity recovery distance d_{rec}/L_x is of the order of 20.

Meteorological parameters include geostrophic velocity, geostrophic height and surface roughness length. Figure 11 shows the impact of the geostrophic velocity for the hypothetical wind farm for hub height velocities near cut-in, halfway cut-in and nominal, near nominal, halfway between nominal and cut-out, and beyond cut-out. The relative initial velocity deficit $(W_{\text{ups}} - W_{\text{ini}})/W_{\text{ups}}$ is found to decrease with increasing geostrophic velocity, and the largest absolute initial velocity deficits $W_{\text{ups}} - W_{\text{ini}}$ (of in this case 1.2 m/s) occur when the hub-height velocity is halfway cut-in and nominal. Also the relative velocity recovery distance is found to increase with the geostrophic velocity, from 0 at low geostrophic velocities to a limit value near 40 at high geostrophic velocities.

6. Summary

A validation of the dedicated planetary boundary layer method MFwWF has been presented on basis of wakes measured downstream of the Horns Rev and the Nysted wind farms. The calculated decrease of the relative velocity deficit with increasing distance behind a wind farm is shown to be supported by data measured in both wind farms. On the other hand, the measured data is shown to be inconclusive as to the calculated decrease of this deficit with increasing upstream velocity. In addition it has been shown that quantitative conclusions can not be drawn because the spanwise positions where the calculations and the measurements are evaluated are different. May this be as it is, it has been shown that in a qualitative sense the calculated relative velocity deficits are in agreement with the measured ones.

Resolved profiles have been presented that show how most of the velocity change occurs in the lower part of the atmospheric boundary layer whereas most of the wind direction change occurs in the upper part. The profiles also show that the thinner the boundary layer or the larger the surface roughness, the larger the wind direction change. Furthermore it has been shown that near

a wind turbine with a rotor diameter of 100 m operating at a full load of 5 MW the velocity deficit is of the order of 5%, the wind direction change is increased with 1...2 deg, and the velocity recovery distance is 20 rotor diameters. And it has been shown that for a wind farm with 22 of these turbines these numbers are 15%, 2...3 deg, and at least 2 wind farm length scales, respectively.

Initial velocity deficits and velocity recovery distances have been presented that show the impact of nominal power density and geostrophic velocity for a wind farm which consists of 22 wind turbines with a nominal power of 5 MW. It has been shown that the initial velocity deficit relative to the upstream velocity decreases with increasing geostrophic velocity in general, and ranges from 6% (at a turbine separation of 14 rotor diameters) to 32% (at a separation of 5 rotor diameters) if the velocity at hub height is halfway cut-in and nominal. Also it has been shown that at this hub-height velocity the absolute initial velocity deficit reaches a maximum (of 1.2 m/s in the case of a nominal power density of 5 MW/km²), and the velocity recovery distance relative to the wind farm length scale is of the order of 20. Finally it has been shown that the relative velocity recovery distance for other geostrophic velocities ranges between 0 (at low geostrophic velocities) and a limit value of the order of 40 (at high velocities).

Acknowledgements

Work funded by the Dutch Ministry of Economic Affairs in BSIK programme We@Sea, project "Windenergiecentrale Noordzee - Parkinteractie" (We@Sea/BSIK 2005/002).

Measured data by courtesy of L.E. Jensen of Dong Energy A/S as prepared in the framework of the European UPWIND research project under contract with the European Commission (CE Contract Number 019945 (SES6)).

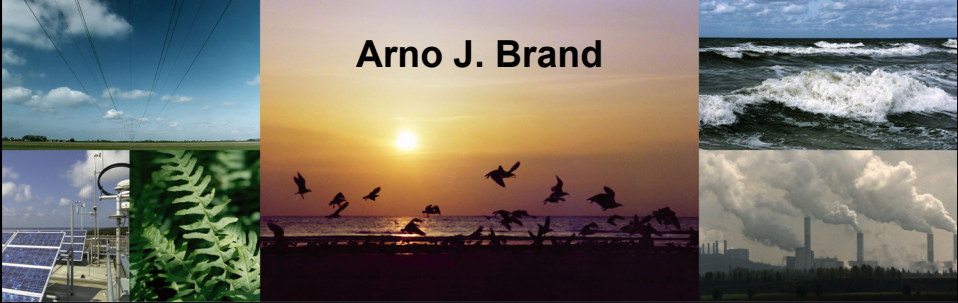
References

- [1] M.B. Christiansen and C.B. Hasager, 2005, "Wake studies around a large offshore wind farm using satellite and airborne SAR", 31st Int. Symp on Remote Sensing of Environment, St Petersburg, Russian Federation
- [2] A.J. Brand, 2007, "Modelling the effect of wind farming on mesoscale flow - Part 1: Flow model", J. of Physics: Conf. Series 75 (2007) 012043
- [3] A.J. Brand, 2008, "Modelling the effect of wind farming on mesoscale flow - Part 2: Modification of the velocity profile", European Wind Energy Conference 2008, Brussels, Belgium
- [4] A.J. Brand, 2008, "The effect of wind farming on mesoscale flow", Global Wind Energy Conference 2008, Beijing, China
- [5] J.R. Holton, 1992, *An Introduction to*

dynamic meteorology (3rd ed.),
Academic Press

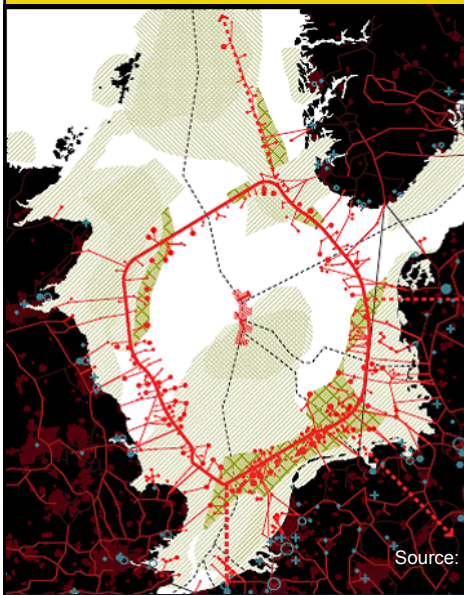
- [6] S. Frandsen et al., 2004, "The necessary distance between large wind farms offshore - Study", Report Risø-R-1518(EN)
- [7] T. Hegberg, 2004, "Turbine interaction in large offshore wind farms - Atmospheric boundary layer above a wind farm", Report ECN-C--04-033
- [8] T. Hegberg, 2002, "The effect of large wind farms on the atmospheric boundary layer", Global Wind Power Conference 2002, Paris, France
- [9] M-K. Liu et al., 1983, "Mathematical model for the analysis of wind-turbine wakes", J. Energy, Vol. 7, No. 1, pp. 73-78
- [10] S. Baidya Roy et al., 2004, "Can large wind farms affect local meteorology?", J. Geoph. Research, Vol. 109, D19101
- [11] P. Rooijmans, 2004, "Impact of a large-scale offshore wind farm on meteorology - Numerical simulations with a mesoscale circulation model", Universiteit Utrecht, Masters thesis
- [12] D.C. Willcox, 1998, *Turbulence modelling for CFD (2nd ed.)*, DCW Industries Inc.

Wind Farm Design When other wind farms are close



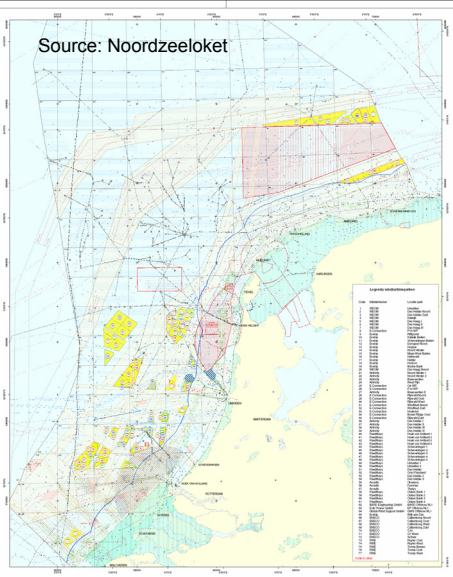
Arno J. Brand

www.ecn.nl



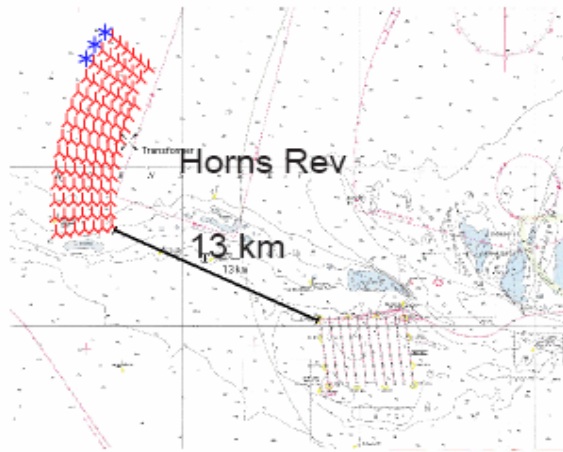
Source: Rem Koolhaas' Office for Metropolitan Architecture (OMA)

Source: Noordzeeloket



Source: Wind Service Holland

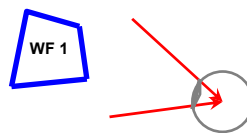
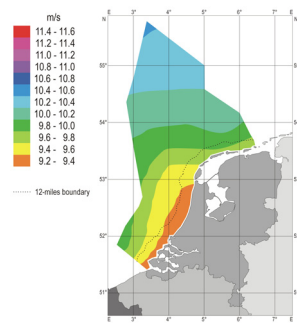




Source: DONG Energy

Large offshore wind farms may affect each other's wind resource

Mean Wind Speed at the Netherlands' Exclusive Economic Zone (NEEZ)
 Period: 1997 - 2002
 Height: 60 m above mean sea level



velocity deficit
 disturbed wind rose

Copyright (c) 2004 by Energy research Centre of the Netherlands, Petten, the Netherlands
 Supported by the Programme 'Duurzame Energie in Nederland' as operated by SenterNovem for the Dutch Ministry of Economic Affairs

Can we design a wind farm when other sites are close?

Can we design a wind farm when other sites are close?

Yes

How?

Can we design a wind farm when other sites are close?

Yes

How?

By determining the local wind climate

How?

Can we design a wind farm when other sites are close?

Yes

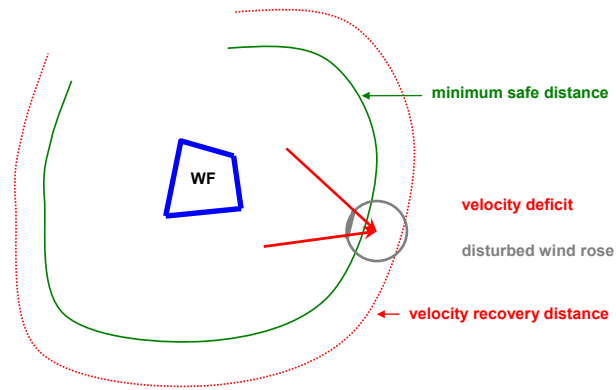
How?

By determining the local wind climate

How?

By modelling planetary boundary layer flow with wind farming

Conclusion



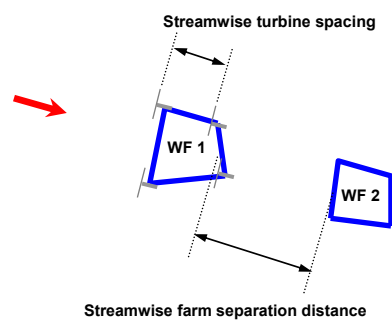
Outline

- ❑ Concepts
- ❑ Approach
- ❑ Validation
- ❑ Predictions

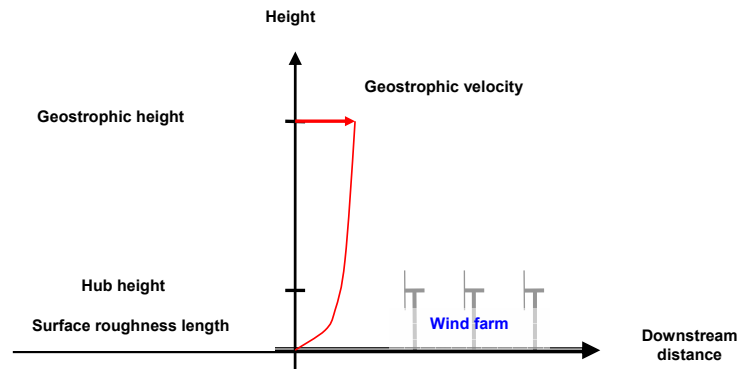
Design parameters

- Wind farm design parameters
 - * Farm separation distance
 - * Turbine spacing
 - * Hub height
 - * Rotor diameter
 - * Nominal power
- Meteorological design parameters
 - * Geostrophic velocity
 - * Geostrophic height
 - * Surface roughness length

Design parameters



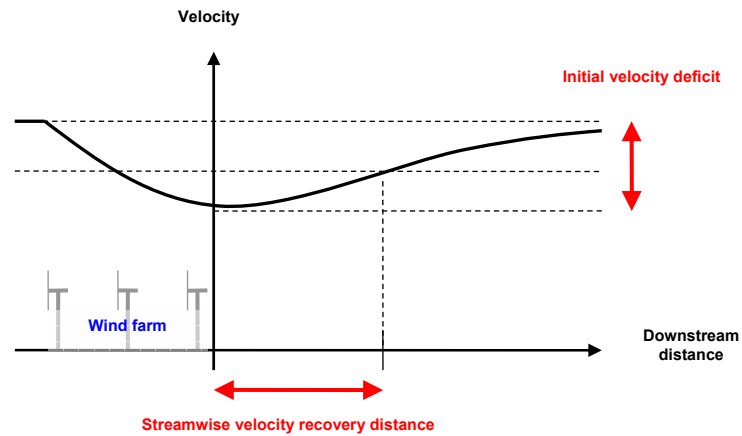
Design parameters



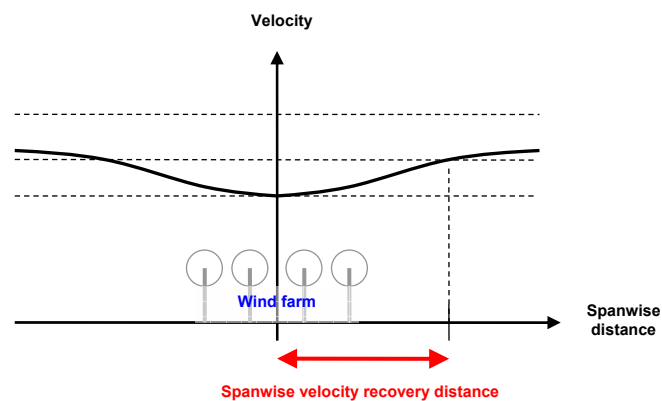
Impact parameters

- Velocity deficit
- Velocity recovery distance
- Minimum safe distance
- Disturbed sectors

Velocity deficits and recovery distances



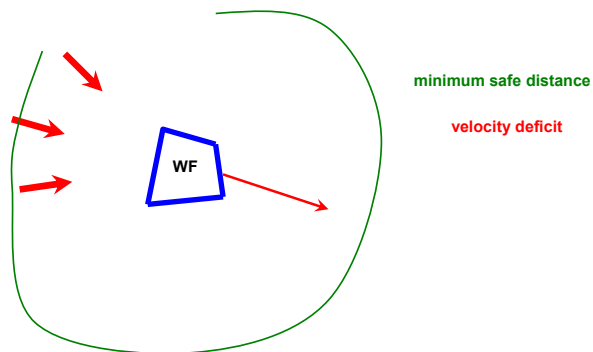
Spanwise recovery distance



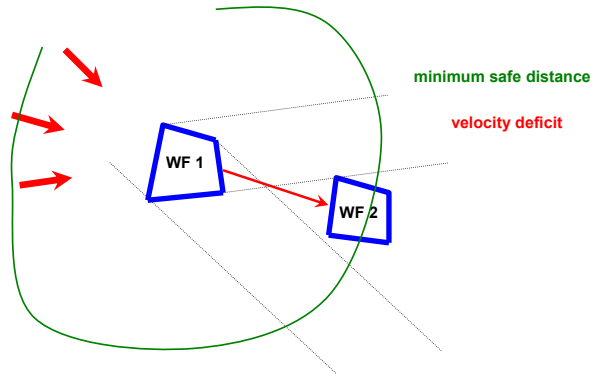
Velocity deficit



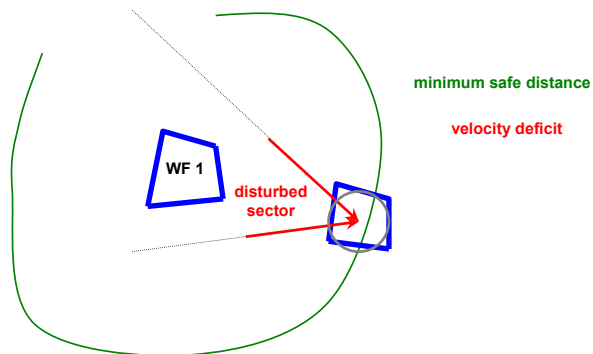
Minimum safe distance



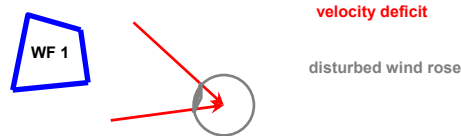
Disturbed sectors



Disturbed sectors



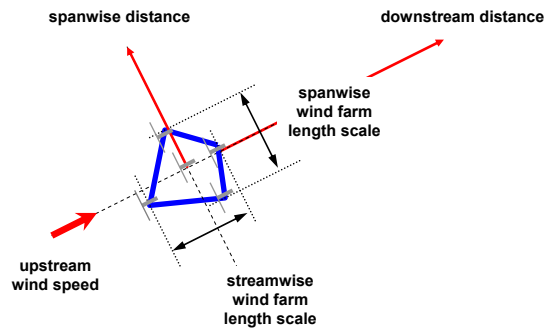
Disturbed wind rose



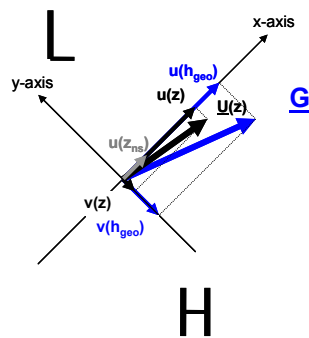
Flow solver

- Neutral planetary boundary layer flow with wind farming
 - * Steady and two-dimensional
 - * Equilibrium between convective and Coriolis forces ...
 - * ... and vertical and spanwise turb. mom. flux gradients ...
 - * ... and forces due to the wind turbines
- Numerical representation
 - * Implicit solution in the vertical
 - * Marching solution in horizontal directions
 - * Implicit Lagrange multiplier velocity correction

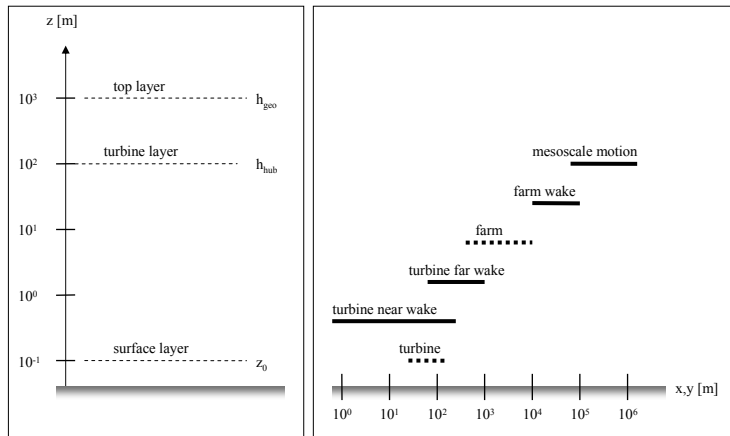
Flow problem



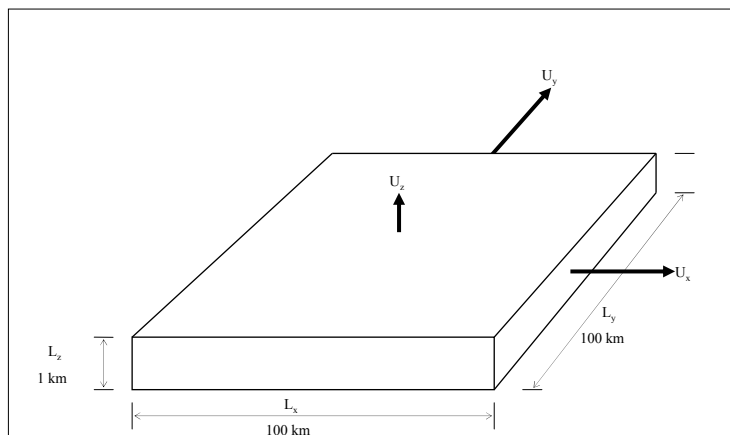
Velocity decomposition



Vertical and horizontal length scales



Length and velocity scales



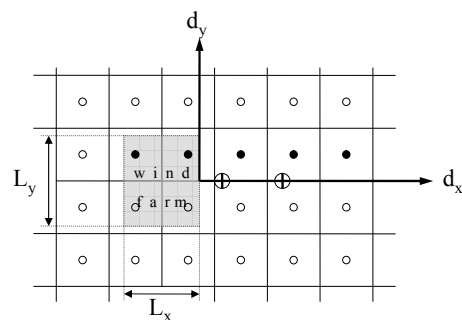
Governing equations

$$\bar{u} \frac{\partial \bar{u}}{\partial x} + \bar{v} \frac{\partial \bar{u}}{\partial y} = +f_\phi (\bar{v} - v_g) - \frac{\partial \bar{u}'v'}{\partial y} - \frac{\partial \bar{u}'w'}{\partial z} + \bar{a}_x$$

$$\bar{u} \frac{\partial \bar{v}}{\partial x} + \bar{v} \frac{\partial \bar{v}}{\partial y} = -f_\phi (\bar{u} - u_g) - \frac{\partial \bar{v}'v'}{\partial y} - \frac{\partial \bar{v}'w'}{\partial z} + \bar{a}_y$$

$$\frac{\partial \bar{u}}{\partial x} + \frac{\partial \bar{v}}{\partial y} = 0$$

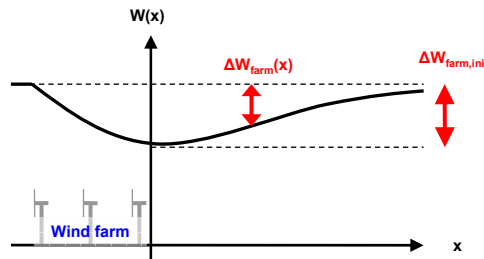
Layout of grid cells



- grid point (centre of cell)
- grid point where calculated velocity is evaluated
- ⊕ point where measured velocity is evaluated

Decay of velocity deficit

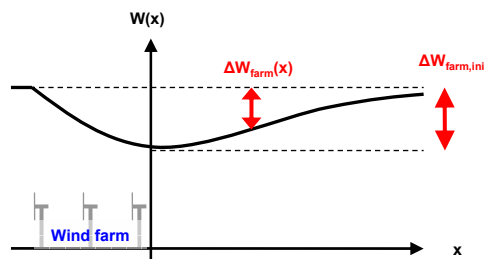
$$\frac{\Delta W_{farm}(x)}{\Delta W_{farm,ini}} = \left(\frac{x}{2D_{rot}} \right)^m$$



Inspiration: R.J. Barthelmie et al., 2008, EWEC 2008, Brussels, Belgium

Decay of velocity deficit

$$\frac{\Delta W_{farm}(x)}{\Delta W_{farm,ini}} = \left(\frac{x}{2D_{rot}} \right)^m$$



$\Delta W_{farm,ini}$ and m
from
calculations
and
measurements

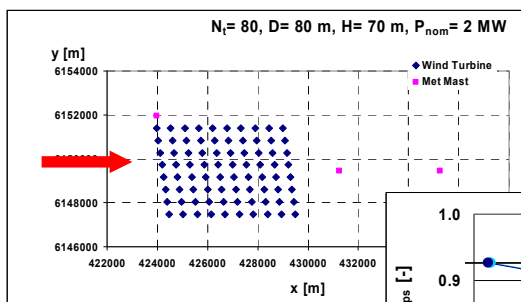
Inspiration: R.J. Barthelmie et al., 2008, EWEC 2008, Brussels, Belgium

Grid-cell versus one-point velocities

Translation

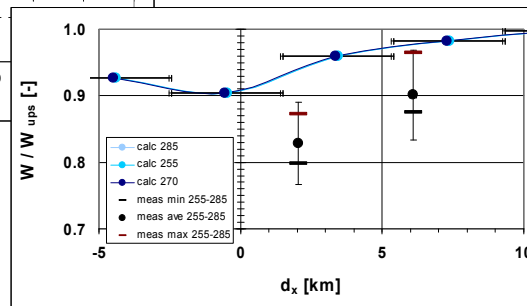
$$\overline{W_{\text{cell}}(x_1, x_2)} = W_0 - f(m, \Delta W_{\text{ini}}; N_t, D, x_1, x_2, \Delta y)$$

Horns Rev wind farm



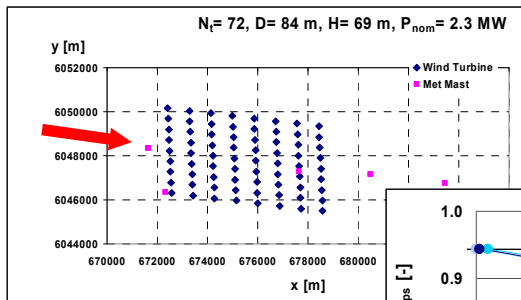
Grid-cell values

One-point values



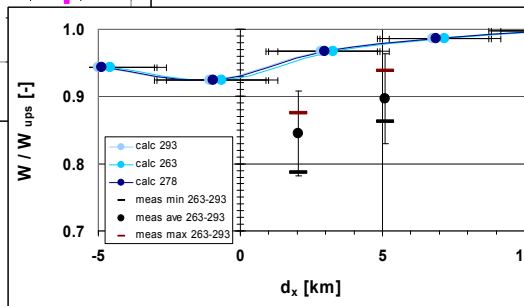
Source: DONG Energy

Nysted wind farm



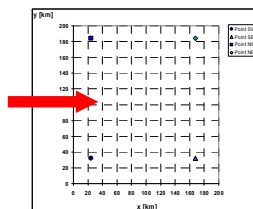
Grid-cell values

One-point values



Source: DONG Energy

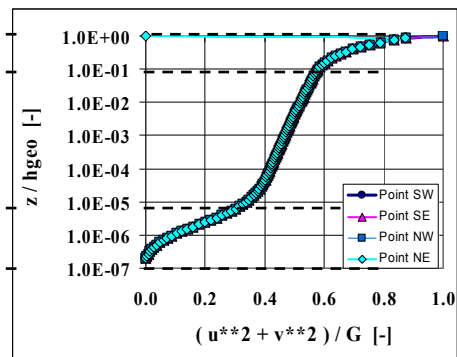
Velocity profile without a wind farm



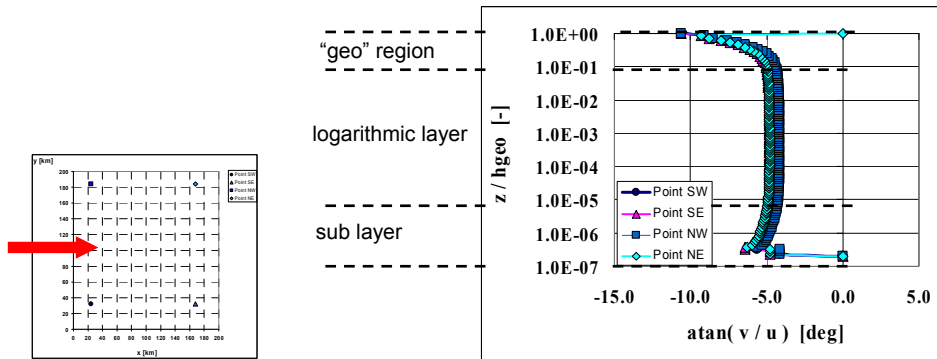
"geo" region

logarithmic layer

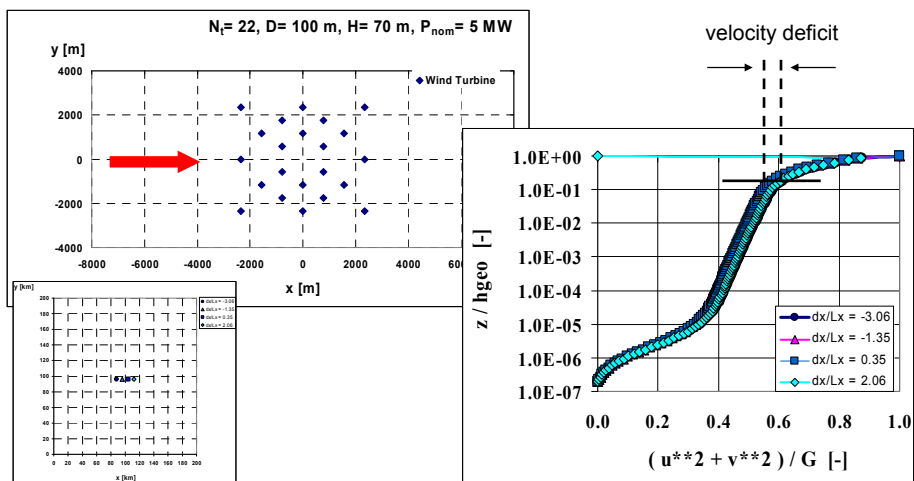
sub layer



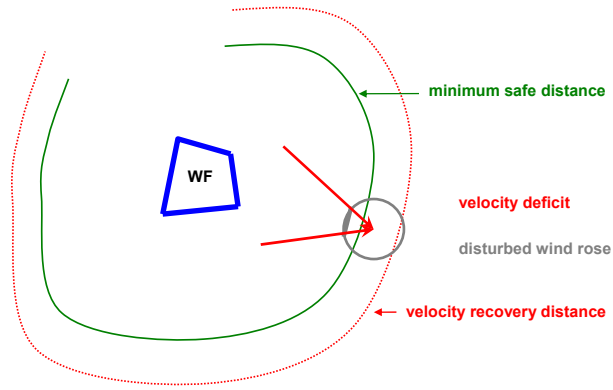
Velocity profile without a wind farm



Velocity profile near a hypothetical wind farm



Conclusion



Extra

Momentum equations ...

- ❑ Discretisation
- ❑ Representation
- ❑ Solution procedure
- ❑ Formal order of method
- ❑ Numerical stability
- ❑ Conservation of mass and energy

Other aspects

- ❑ Lagrange-multiplier approach
- ❑ Turbulence parameterization
- ❑ Wind turbine parameterization
- ❑ Initial and boundary conditions
- ❑ Discretization error estimation

Impact of nominal power density on initial velocity deficit**Impact of nominal power density on velocity recovery distance**

Summary